Iranian Journal of Medical Physics

ijmp.mums.ac.ir

Simulation Study on the Effect of High-Intensity Focused Ultrasound on Thermal Lesion of Biological Tissue under Different Treatment Modes

Hu Dong[1*], Gang Liu[1,2], Zhenzhong Ma[1], Gaofeng Peng[1], Ping Pan[1]

1. School of Information Science and Engineering, Changsha Normal University, Changsha 410100, China
2. School of Physics and Electronics, Central South University, Changsha 410083, China

ARTICLE INFO

Article type:
Original Paper

Article history:
Received: Aug 05, 2021
Accepted: Feb 08, 2022

Keywords:
High-intensity Focused Ultrasound
Treatment Interval
Lesion Area
Intermittent Treatment

ABSTRACT

Introduction: High-intensity Focused Ultrasound (HIFU) treatment is a non-invasive technology. The purpose of this study was to explore the effects of different treatment depths, tissue types and treatment interval on biological tissue thermal lesions under continuous and intermittent treatment modes.

Material and Methods: A simulation model of biological tissue irradiated by HIFU was established by finite difference time domain (FDTD). The thermal lesion of biological tissue irradiated by HIFU was calculated using the spherical beam equation (SBE) and Pennes biological heat transfer equation (PBHTE). Parameters such as treatment depth, tissue type, and treatment interval were varied to explore their effects on the thermal lesion to biological tissues in both continuous and intermittent treatment modes.

Results: For the same biological tissue or treatment depth, with the increase of HIFU irradiation time, the focal temperature under continuous treatment was higher than that under intermittent treatment, and the thermal lesion area under continuous treatment was greater than that under intermittent treatment. Whether continuous or intermittent treatment, with the increase of treatment depth, the temperature rise rate of deep tissue was slower than that of superficial tissue, and the thermal lesion area decreased gradually. Moreover, in the intermittent treatment mode with a long single treatment time and short treatment interval, the focal temperature rase quickly and the thermal lesion area was large.

Conclusion: For the same tissue type, treatment depth, or any treatment interval, the focal temperature and thermal lesion area corresponding to continuous treatment were greater than those corresponding to intermittent treatment.

►*Please cite this article as:*
Dong H, Liu G, Ma Zh, Peng G, Pan P. Simulation Study on the Effect of High-Intensity Focused Ultrasound on Thermal Lesion of Biological Tissue under Different Treatment Modes. Iran J Med Phys 2022; 19: 199-206. 10.22038/IJMP.2022.59497.1999.

Introduction

High-intensity focused ultrasound (HIFU) is a non-invasive tissue hyperthermia method, which has attracted much attention in the field of medical treatment for decades [1-4]. HIFU device is being studied as an effective method for the treatment of solid tumors such as prostate, liver, breast, kidney, and brain [5-8]. Because HIFU irradiation can rapidly raise the temperature at the focus to more than 60 ℃, so that the tumor can be ablated within a few seconds without damaging the surrounding tissue.

In the existing clinical HIFU equipment, there are two modes of ultrasonic energy transmission, namely continuous treatment mode and intermittent treatment mode [9-10]. The former strategy is to irradiate biological tissue continuously for a short period of time without interruption. However, the latter is that each ultrasonic irradiation is conducted for a short time (usually 2~8 s), and then suspended for a short period of time (usually 1~5 s) for several times. In order to better understand the physical mechanism of HIFU treatment, numerical simulation was carried out to study the formation of a thermal lesion in tissue, the thermal lesion area, and HIFU treatment efficiency under continuous treatment mode and intermittent treatment mode were compared with each other.

Zhang, and et al [10] compared the effects of HIFU continuous irradiation and discrete irradiation on porcine liver lesion, and they found that compared with the traditional discrete treatment scheme, continuous irradiation can produce more uniform lesions in tissue and significantly reduce the total treatment time. Fan, and et al [11] used two energy transfer strategies of HIFU continuous scanning and discrete scanning to conduct numerical simulation and experimental research on the lesion formation and temperature distribution induced by HIFU. It was found that the peak temperature distribution and lesion boundary were more uniform in the continuous scanning mode.

Wang, and et al [12] used a 60% pulse duty cycle, pulse duration of 6ms, and total irradiation time of 5 s

*Corresponding Author: Tel: +86-0731-84036108; E-mail: wjd3203@163.com

to compare the ablation effect of continuous pulse therapy in bovine liver and rabbit liver. Xu, and et al [13] used the irradiation mode of fixed-point irradiation for 2 s, stopping for 2~3 s and irradiation for 1~6 times to judge the ablation of the target area according to whether the focal temperature of magnetic resonance imaging (MRI) temperature map reaches 60 ℃~65 ℃. Yi, and et al [14] also used MRI-guided HIFU treatment equipment to treat 44 symptomatic hysteromyomas of 43 patients with ultrasound treatment by irradiating for 2 s and stopping for 2~3 s, which verified the feasibility and safety of MRI-guided HIFU in the treatment of hysteromyomas.

In this paper, the finite difference method is used to construct the simulation model of biological tissue irradiated by HIFU. Combined with the spheroidal beam equation (SBE) and Penne's biological heat transfer equation (PBHTE), the thermal lesion of biological tissue irradiated by HIFU is calculated. The thermal lesion of biological tissue under different tissue types, treatment depth, and treatment interval under continuous and intermittent HIFU treatment modes is simulated, and the laws between the change of these parameters and the change of focal temperature and thermal lesion area are discussed. The research results are expected to provide theoretical reference for the formulation of a safe and effective preoperative treatment scheme for HIFU.

Materials and Methods

SBE

Khokhlov-Zabolotskaya-Kuznetsov (KZK) equation was used to calculate the sound field of ultrasonic transducer based on parabola approximation [15], so it was only applicable to transducers with half aperture angle <16°(half of transducer aperture angle), while Westervelt equation took a relatively long time [16-18]. Therefore, the SBE equation was used to calculate the sound field of HIFU, and it was also used to describe the propagation of nonlinear ultrasound in an ellipsoidal coordinate system, where $-\infty<\sigma<\infty$, $0\le\eta\le1$, $0\le\varphi<2\pi$ (Figure 1).

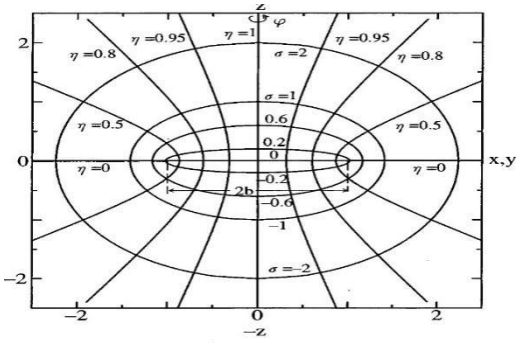

Figure 1. Oblate spherical coordinate system

The transformation relationship between the ellipsoidal coordinate system (σ,η,φ) , and a rectangular coordinate system (x,y,z) is: $x=b[(1+\sigma^2)(1-\eta^2)]^{1/2}\cos\varphi$, $y=b[(1+\sigma^2)(1-\eta^2)]^{1/2}\sin\varphi$, $z=b\sigma\eta$, $\eta=\cos\theta$, $2b$ is the focal length.

The SBE equation divides the focused ultrasonic field into two regions, the spherical wave approximation region near the surface of the transducer ($\sigma<\sigma_0$) and the plane wave approximation region near the focal ($\sigma>\sigma_0$). For the spherical wave approximation region

$$\frac{\partial^2P}{\partial\tau_s\partial\sigma}+\frac{1}{2}\frac{\sin2\theta}{\sigma(1+\sigma^2)}\frac{\partial^2P}{\partial\tau_s\partial\theta}+\frac{\varepsilon\sqrt{\sigma^2+\sin^2\theta}}{\sigma(1+\sigma^2)}\left(\frac{\partial^2P}{\partial\theta^2}+\cot\theta\frac{\partial P}{\partial\theta}\right)=-\frac{E}{\sigma}\frac{\partial P}{\partial\tau_s}-\frac{\sqrt{\sigma^2+\sin^2\theta}}{\sigma}\left(\alpha b\frac{\partial^3P}{\partial\tau_s^3}+\frac{b}{2l_D}\frac{\partial^2P^2}{\partial\tau_s^2}\right)E \quad (1)$$

Where $P=p/p_0$ is the standardized sound pressure, $\alpha=\delta\omega^2/(2c_0^3)$ is the sound attenuation coefficient, δ、ω and c_0 are the sound diffusivity, angular frequency, and sound velocity in the medium, respectively. $l_D=\rho_0c_0^3/(p_0\beta\omega)$ is the impact formation distance of plane wave, and ρ_0、p_0 ,and β are the density of the medium, the amplitude of sound pressure on the surface of the transducer, and nonlinear coefficient, respectively. $\beta=1+(B/2A)$, and B/A is the ratio of the second-order (B) coefficients to the first-order (A) coefficients of the Taylor series expansion [19]. $\varepsilon=1/(2kb)$, k , and b are the wave number and half inner focal length, respectively, $\tau_s=\omega[t+b(\sigma^2+\sin2\theta)^{1/2}/c_0$. In the above formula, E is a function of σ , and θ , expressed as

$$E(\sigma,\theta)=\frac{\sigma^2+\cos^2\theta}{1+\sigma^2} \quad (2)$$

The plane wave approximation region can be expressed as:

$$\frac{\partial^2P}{\partial\tau_p\partial\sigma}-\frac{\sigma\sin\theta}{1+\sigma^2}\frac{\partial^2P}{\partial\tau_p\partial\theta}-\frac{\varepsilon(2-\cos\theta)}{1+\sigma^2}\left(\frac{\partial^2P}{\partial\theta^2}+\cot\theta\frac{\partial P}{\partial\theta}\right)=\left(ab\frac{\partial^3P}{\partial\tau_p^3}+\frac{b}{2l_D}\frac{\partial^2P^2}{\partial\tau_p^2}\right)E \quad (3)$$

$\tau_p=\omega[t-b\sigma\cos\theta/c_0]$, due to the axial symmetry of the spherical shell coordinate system, the variable φ is omitted from above equation. Equations (1) and (3) are solved by the combination of the time domain and frequency domain. Using operator separation, equations (1) and (3) can be simplified as follow:

$$\frac{\partial^2 \bar{P}}{\partial \bar{\tau} \partial \sigma} = G(\sigma,\theta)\frac{\partial^2 P}{\partial \bar{\tau} \partial \theta} + H(\sigma,\theta)\left(\frac{\partial^2 P}{\partial \theta^2} + \cot\theta \frac{\partial P}{\partial \theta}\right) + R(\sigma,\theta)\frac{\partial P}{\partial \tau} + S(\sigma,\theta)\frac{\partial^3 P}{\partial \tau^3} \quad (4)$$

$$\frac{\partial P}{\partial \sigma} = N(\sigma,\theta)\frac{\partial P^2}{\partial \tau} \quad (5)$$

The coefficients $G(\sigma,\theta)$, $H(\sigma,\theta)$, follow $R(\sigma,\theta)$, $S(\sigma,\theta)$ and $N(\sigma,\theta)$ can be derived from equations (1) and (3). Equation (4) contains diffraction and attenuation terms, which are calculated by the traditional frequency domain algorithm [20]. Equation (5) is a nonlinear term, which is calculated by the time-domain difference algorithm [21-23].

PBHTE

The PBHTE is used to simulate thermal lesion, which is expressed as [24,25]

$$\rho_t C_t \frac{\partial T}{\partial t} = K_t \nabla^2 T - W_b C_b (T - T_b) + Q_v \quad (6)$$

In formula (6), ρ_t and C_t are the density and specific heat capacity of the medium, respectively. The first term on the right is the heat conduction term, and K_t is the heat conduction coefficient of biological tissue. The second item on the right is perfusion cooling, where W_b 、 C_b 、 T and T_b are the perfusion coefficient of the blood flow, the specific heat capacity of blood, the temperature of biological tissue, and the temperature of blood in the heating zone, respectively. The third item on the right is the heat accumulation absorbed by the tissue when ultrasound propagates through the medium. The heat accumulation caused by the sound field can be expressed as [24]:

$$Q_v = 2\alpha I \quad (7)$$

α is the attenuation coefficient of tissue, and I is sound intensity in the focal region of transducer, the PBHTE is solved by finite difference time domain (FDTD) method [26].

Equivalent heat dose

The calculation formula of equivalent heat dose TD_{43} [15,27] is calculated by formula (8).

$$TD_{43} = \int_0^t R^{43-T(t)} dt \quad (8)$$

In formula (8), R is a constant. When $T \geq 43$ ℃, R=0.5, and when T <43 ℃, R=0.25. In this paper, the lesion area where the equivalent heat dose is greater than 240 min is defined as the area of thermosetting necrosis.

Numerical simulation model and simulation parameters

Numerical simulation model

A two-dimensional axisymmetric simulation model of HIFU irradiated biological tissue was established, as shown in Figure 2. The simulation area was composed of the ultrasonic transducer, water environment and in vitro tissue model. A perfect matching layer was added at the boundary of the model to avoid the influence of reflection and diffraction on the sound field in the target area. The z-axis is the ultrasonic propagation direction, and the r-axis is the radius direction of the transducer. In order to simplify the problem analysis, this study ignored the effect of cavitation on focal temperature and lesion of biological tissue.

HIFU source was a concave spherical ultrasonic transducer with frequency f =1.0 MHz, geometric focal length F = 6.0 cm, outer radius a =2.5 cm, inner radius [28] b =1.0 cm. The output power of the transducer and the treatment depth d_l can be adjusted. The spatial grid parameters used for simulation are dz=0.068 mm and dr=0.089 mm. The nonlinear harmonic order was 128, and the time steps of the sound field and temperature field were 6×10^{-9} s and 0.002 s, respectively. The presented method was evaluated on an Intel (R) core (TM) i7-9750H CPU @ 2.60 GHz with 8.0 GB RAM PC using Windows 10 operating system, and MATLAB R2011 (MathWorks, Natick, Massachusetts, United States) software was used to simulate biological tissue thermal lesion.

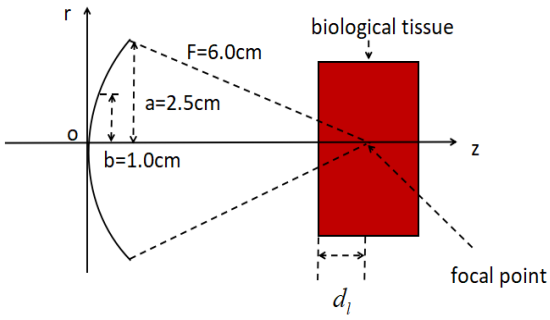

Figure 2. Geometric model of biological tissue irradiated by HIFU

The simulation consists of an acoustic module and a thermal module. Firstly, the acoustic module is calculated to extract the sound intensity I in the focal region of the transducer to obtain Q_v. For intermittent treatment mode, we set the treatment interval function of HIFU irradiated biological tissue as $M_i(t)(i=1,2,3)$.

Table 1. Acoustic and thermal parameters of different medium [26,29-33]

Material	ρ_0(kg/m^3)	c_0(m/s)	α(dB/m)	B/A	C_t(J/kg/K)	K_t(W/m/K)
Water	1000	1482	0.217	5.0	4180	0.60
Skin	1109	1400	115	7.0	3530	0.40
Fat	960	1476	36	10.3	2973	0.24
Liver	1036	1590	58	6.6	3604	0.53

$M_1(t)$: 1.2 s-2.8 s-4 number, indicating that the treatment time was 1.2 s, the treatment interval was 2.8 s, and the number of treatment was 4. $M_2(t)$: 1.6 s-2.4 s-4 number, indicating that the treatment time was 1.6 s, the treatment interval was 2.4 s, and the number of treatment was 4. $M_3(t)$: 2.0 s-2.0 s-4 number, indicating that the treatment time was 2.0 s, the treatment interval was 2.0 s, and the number of treatment was 4. For continuous treatment mode, the treatment interval was 0 s. In the thermal module, $Q_v.M_i(t)$ is loaded into the focal region as the heat source to calculate the temperature change and thermal lesion of tissue under different treatment modes.

Simulation parameters

The parameters of water and biological tissue used in the calculation are shown in Table 1.

Results

Effect of tissue type on thermal lesion

Kept the treatment depth d_l =1 cm and treatment interval unchanged to explore the effects of different tissue types on focal temperature and thermal lesion under continuous mode and intermittent treatment mode $M_3(t)$. Figure 3 and Figure 4 showed the temperature rise and thermal lesion area of HIFU focus under different tissue types. It can be seen from Figure 3 that under the same irradiation condition, whether continuous irradiation or intermittent irradiation, the focal temperature of the liver was the lowest and the focal temperature of the skin was the highest, the temperature rise rate of the liver was the slowest and the temperature rise rate of the skin was the fastest. For the same tissue, the focal temperature difference between continuous and intermittent irradiation was slight shortly after HIFU irradiation. With the increase in HIFU irradiation time, the focal temperature under continuous irradiation was higher than that under intermittent irradiation. In the intermittent irradiation mode, it took about 14 s for the liver to achieved the maximum temperature, while it took about 6 s, and 2 s for fat and skin to reach the same temperature, which was shortened by about 4/7, and 6/7, respectively. The thermal lesion distribution of the skin, fat, and the liver was shown in Figure 4. Under continuous or intermittent irradiation, the thermal lesion area of the skin was the largest and that of the liver was the smallest. For the same tissue, the thermal lesion area corresponding to continuous irradiation was more significant than that corresponding to intermittent irradiation. The thermal lesion area was calculated quantitatively by Photoshop software [34]. The corresponding thermal lesion area of the liver, fat and the skin under continuous irradiation were 1.04 cm^2, 1.12 cm^2, and 1.78 cm^2, respectively, and the corresponding thermal lesion area of the liver, fat and the skin under intermittent irradiation were 0.52 cm^2, 0.61 cm^2, and 1.11 cm^2, respectively.

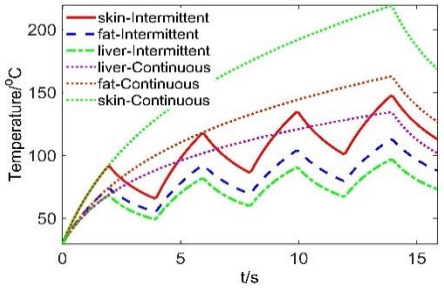

Figure 3. Comparison of focal temperature in different tissue

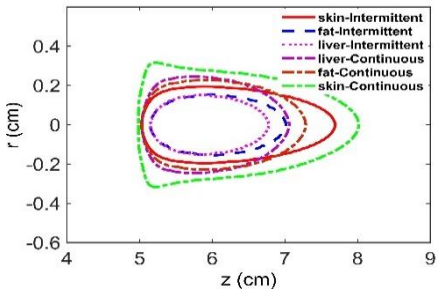

Figure 4. Comparison of lesion area in different tissue

Effect of treatment depth on thermal lesion

Kept the tissue type as liver and the treatment interval unchanged to explore the effects of different treatment depths on focal temperature and thermal lesion under continuous mode and intermittent treatment mode $M_3(t)$. It can be seen from Figure 5 that under the same treatment interval, with the increase of treatment depth, the focal temperature rise of deep tissue was smaller than superficial tissue at the end of treatment, regardless of treatment mode. Moreover, the temperature rise rate of deep tissue was slower than superficial tissue. For the same treatment depth, the focal temperature difference between continuous irradiation and intermittent irradiation was slight shortly after the beginning of HIFU irradiation. With the increase in HIFU irradiation time, the focal temperature under continuous irradiation was higher than that under intermittent irradiation. Figure 6 showed that the lesion area gradually decreased with the depth of irradiation under

different thermal treatments, whether continuous or intermittent treatment mode. For the same treatment depth, the thermal lesion area corresponding to continuous irradiation was more significant than that corresponding to intermittent irradiation. The thermal lesion area corresponding to the treatment depth of 3 cm, 2 cm, and 1 cm under continuous irradiation were 0.63 cm^2, 0.74 cm^2, and 0.93 cm^2, respectively, and the thermal lesion area corresponding to the treatment depth of 3 cm, 2 cm and 1 cm under intermittent irradiation were 0.31 cm^2, 0.42 cm^2, and 0.52 cm^2, respectively.

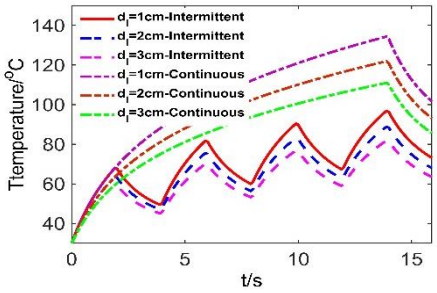

Figure 5. Comparison of focal temperature at different depth

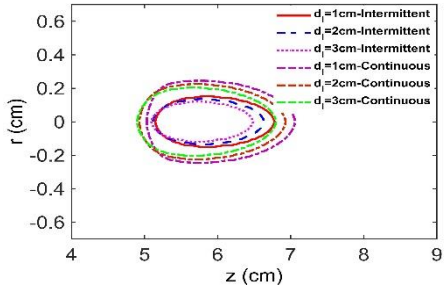

Figure 6. Comparison of lesion area at different depth

Effect of treatment interval on thermal lesion

Kept the tissue type as liver and treatment depth d_l =2 cm unchanged to explore the effect of treatment interval on focal temperature rise and thermal lesion under continuous and intermittent treatment modes. Figure 7 shows focal temperature rise in the liver under four different treatment intervals. Shortly after the beginning of HIFU irradiation, the corresponding focal temperature difference between continuous and intermittent irradiation was slight, but with the gradual increase of irradiation time, the focal temperature under continuous irradiation was gradually higher than that under intermittent irradiation. The intermittent treatment mode $M_3(t)$ with a long single treatment time and short interval had the fastest temperature rise, while the intermittent treatment mode $M_1(t)$ with short single treatment time and long interval had the slowest temperature rise. Figure 8 showed the comparison of thermal lesion area of the liver under intermittent mode and continuous treatment mode. The thermal lesion area under continuous irradiation was more significant than that under intermittent irradiation. For the thermal lesion under the intermittent treatment mode corresponding to three different treatment intervals, due to the long diffusion time of heat to surrounding tissue, the long single treatment time and a short interval under intermittent treatment mode $M_3(t)$, the corresponding thermal lesion area was larger. The heat diffusion time to the surrounding tissue in the intermittent treatment mode $M_1(t)$ with short single treatment time and long interval was relatively short, so the corresponding thermal lesion area was small. The thermal lesion area corresponding to continuous treatment mode and three intermittent treatment modes $M_1(t)$、$M_2(t)$ and $M_3(t)$ were 0.78 cm^2 ,0.21 cm^2, 0.33 cm^2, and 0.36 cm^2 , respectively.

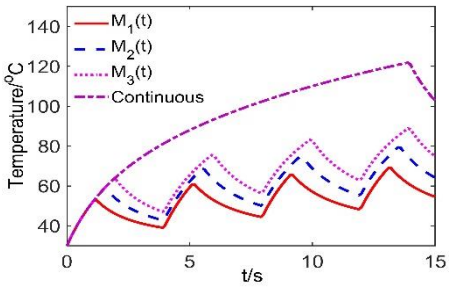

Figure 7. Comparison of focal temperature under different treatment intervals

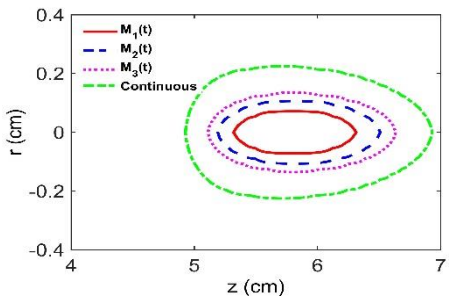

Figure 8. Comparison of lesion area under different treatment intervals

Discussion

Under the same conditions, whether continuous treatment mode or intermittent treatment mode, due to the difference in acoustic parameters such as density, sound velocity and attenuation coefficient of different tissue, as well as thermal parameters such as thermal conductivity and thermal diffusion coefficient, the energy attenuation of ultrasound in the process of sound channel propagation was different, resulting in the difference of energy deposition in the target area [35-37], to affect the temperature rise, and thermal lesion area of tissue. The results showed that the liver had the slowest temperature rise and the lowest focal temperature, and the skin had the fastest temperature rise and the highest focal temperature, which may cause the skin layer to be burned during treatment. Because the attenuation coefficient of the skin was more significant than that of fat and the liver [29-31], and the ultrasonic energy absorbed by skin layer was greater than that absorbed by fat and liver under the same condition, the thermal lesion area of skin was the largest and the lesion area of

liver was the smallest. At this moment, the ultrasonic coupling gel should be applied to the skin surface to reduce the attenuation of the incident ultrasound [38,39]. For the same tissue, the focal temperature under continuous treatment was higher than that under intermittent treatment. Similarly, the thermal lesion area under continuous treatment was larger than that under intermittent treatment.

With the increase of treatment depth, the ultrasonic energy transmitted to the focal gradually decreased due to reflection, scattering, and attenuation [40,41]. The temperature rise rate of superficial tissue was higher than that of deep tissue, and the thermal lesion area gradually decreased with the increase of depth. For the same treatment depth, with the rise in treatment time, the focal temperature under continuous treatment was higher than that under intermittent treatment, and the thermal lesion area corresponding to continuous therapy was more significant than that corresponding to intermittent therapy. For the treatment of deep tumors, the intermittent treatment mode with long single treatment time and short time interval can be switched according to the treatment situation of tumors. In this way, more energy can be concentrated at the focus to eliminate tumors, or consider the use of microbubble contrast agent to increase the deposition of deep ultrasound energy. Microbubble contrast agent can increase the local accumulation of ultrasonic energy by enhancing the biological effect of ultrasound and the ability of target tissue to disperse and reflect ultrasound [42,43], thereby enhancing the thermal lesion effect of HIFU on deep tissue.

Furthermore, the treatment interval had an essential effect on the thermal lesion area of biological tissue during HIFU treatment. Under the same treatment condition, the thermal lesion area under continuous treatment mode was significantly larger than that under intermittent treatment mode. For intermittent treatment mode, single treatment time, treatment interval and treatment times significantly effects on focal temperature and thermal lesion. Overall, in the early stage of HIFU clinical, surgical treatment, continuous treatment mode is a better method for the treatment of large tumor tissue, which can reduce the treatment time and reduce the discomfort and pain caused by patients in the treatment process. However, in the later stage of HIFU clinical, surgical treatment, for small tumor tissue, the intermittent treatment mode with a short single treatment time and the long interval is better. It can effectively control the irradiation dose of HIFU, and reduce the risk of the lesion to healthy tissue and avoid unnecessary the lesion to normal tissue around tumor tissue.

Conclusion

In the simulation study of this paper, we established the theoretical simulation model of thermal lesion of biological tissue irradiated by HIFU. We showed the effects of continuous treatment mode and intermittent treatment mode with different treatment depth, tissue type and treatment interval on biological tissue thermal lesion. In the following research work, we will monitor the thermal lesion of biological tissue through in vitro tissue experiments and MRI-guided HIFU treatment equipment. Combined with the above theoretical model, we will deeply explore the impact of HIFU on the thermal lesions of biological tissue, provide reference ideas for clinical treatment of HIFU and improve the treatment efficiency of HIFU.

Acknowledgment

This work was supported by the Key Project of Hunan Provincial Department of Education of China under grant No. 21A0618, and the Changsha Natural Science Foundation Project under grant No. kq2202313. The authors sincerely thank the anonymous reviewers for their helpful comments and suggestions.

References

1. Khokhlova TD, Hwang JH. HIFU for palliative treatment of pancreatic cancer. Advances in Experimental Medicine & Biology. 2016; 880(3):83-95. DOI:10.1007/978-3-319-22536-4_5.
2. Maloney E, Hwang J H. Emerging HIFU applications in cancer therapy. International Journal of Hyperthermia the Official Journal of European Society for Hyperthermic Oncology North American Hyperthermia Group. 2015; 31(3):302-9. DOI: 10.3109/02656736.2014.969789.
3. Gui F, Zheng H, Li Y, Tan J, Du Y. Simulation research on temperature distribution in focal region during high intensity focused ultrasound intermittent treatment. Journal of Applied Acoustics. 2021;1- 12. DOI: 10.11684/j.issn.1000-310X.2021.03.009.
4. Dom SM, Razak HR, Zaiki FW, Saat NH, Abd Manan K, Isa IN, et al. Ultrasound exposure during pregnancy affects rabbit foetal parathyroid hormone (PTH) level. Quantitative Imaging in Medicine & Surgery. 2013;3(1):49-53. DOI: 10.3978/j.issn.2223-4292.2013.02.06.
5. Orsi F, Arnone P, Chen W, Zhang L. High intensity focused ultrasound ablation: A new therapeutic option for solid tumors. Journal of Cancer Research & Therapeutics. 2010;6(4):414. DOI:10.4103/ 0973-1482.77064.
6. Fura U, Kujawska T. Selection of Exposure Parameters for a HIFU Ablation System Using an Array of Thermocouples and Numerical Simulations. Archives of Acoustics. 2019; 44(2): 349-55.DOI: 10.24425/aoa.2019.128498.
7. Chen C, Wang Y, Tang Y, Wang L, Jiang F, Luo Y, et al. Bifidobacterium-mediated high-intensity focused ultrasound for solid tumor therapy: comparison of two nanoparticle delivery methods. International Journal of Hyperthermia. 2020; 37(1): 870-8. DOI: 10.1080/02656736.2020.1791365.
8. Sazgarnia A, Shanei A, Taheri AR, Meibodi NT, Eshghi H, Attaran N, et al. Therapeutic Effects of Acoustic Cavitation in the Presence of Gold Nanoparticles on a Colon Tumor Model. Journal of Ultrasound in Medicine. 2013; 32(3): 475-83.DOI:10.7863/ jum.2013.32.3.475.
9. Haar DGT, Coussios C. High intensity focused ultrasound: Physical principles and devices. Int J

Hyperthermia. 2007; 23(2):89-104. DOI:10.1080/02656730601186138.
10. Zhang Z, Chen T, Zhang D. Lesions in Porcine livers tissues created by continuous high intensity ultrasound exposures in vitro. Chinese Physics Letters. 2013; 30(2):024302. DOI:10.1088/0256-307X/ 30/2/ 024302.
11. Fan T, Liu Z, Zhang D, Tang M. Comparative study of lesions created by high-intensity focused ultrasound using sequential discrete and continuous scanning strategies. IEEE Transactions on Biomedical Engineering. 2013; 60(3):763-769. DOI:10.1109/TBME.2011.2167719.
12. Wang Y, Wang Q, Luo Y, Jiang L, Zeng Z, Gan L, et al. Comparative Study of Pulsed Versus Continuous High-Intensity Focused Ultrasound Ablation Using In Vitro and In Vivo Models. Journal of Ultrasound in Medicine. 2020 Feb;39(2):259-71. DOI: 10. 1002/ jump. 15098.
13. Xu Y, Fu Z, Yang L, Huang Z, Chen WZ, Wang Z. Feasibility, Safety, and Efficacy of Accurate Uterine Fibroid Ablation Using Magnetic Resonance Imaging-Guided High-Intensity focused Ultrasound With Shot Sonication. Journal of Ultrasound in Medicine. 2015; 34(12):2293-303. DOI:10.7863/ultra.14.12080.
14. Yi W, Wang Z B, Xu Y H. Efficacy, Efficiency, and Safety of Magnetic Resonance-Guided High-Intensity focused Ultrasound for Ablation of Uterine Fibroids: Comparison with Ultrasound- Guided Method. Korean Journal of Radiology. 2018; 19(4):724-32. DOI:10.3348/kjr.2018.19.4.724.
15. Gholami M, Haghparast A, Dehlaghi V. Numerical study for optimizing parameters of high intensity focused ultrasound-induced thermal field during liver tumor ablation: HIFU simulator. Iranian journal of medical physics. 2017; 14(1):15-22. DOI:10.22038/ijmp.2017.19268.1176.
16. Kamakura T, Ishiwata T, Matsuda K. A new theoretical approach to the analysis of nonlinear sound beams using the oblate spheroidal coordinate system. The Journal of the Acoustical Society of America. 1999; 105(6): 3083-6. DOI:10.1121/1.424638.
17. Chen W, Wang P, Zhang Z, Deng X, Zhang C, Ju S. Nonlinear ultrasonic imaging in pulse-echo mode using Westervelt equation:a preliminary research. Computer Assisted Surgery. 2019; 24(2):54-61. DOI:10.1080/ 24699322.2019.1649065.
18. Guo C, Yao L, Zheng H, Wang Y, Gao S, Wang X, et al. Finite element simulation of HIFU nonlinear medical ultrasound field. Ninth International Symposium on Precision Mechanical Measurements. International Society for Optics and Photonics. 2019; 11343:113431Y. DOI:10.1117/12.2548855.
19. Sarkar R, Kumar Pandey P, Kundu S, Panigrahi PK. Exact sub and supersonic pressure wave-fronts in nonlinear thermofluid medium. Waves in Random and Complex Media. 2021;1-14. DOI:10.1080/17455030. 2021.1954263.
20. Gu J, Jing Y. Modeling of wave propagation for medical ultrasound: a review. IEEE Transactions on Ultrasonics Ferroelectrics & Frequency Control. 2015; 62(11):1979. DOI:10.1109/ TUFFC.2015. 007034.
21. Chen T, Qiu YY, Fan TB, Zhang D. Modeling of shock wave generated from a strong focused ultrasound transducer. Chinese Physics Letters. 2013 Jul 1;30(7):074302. DOI:10.1088/0256-307X/ 30/7/ 074302.
22. Wu DL, Gao SP, Yao L, Chen J, Zhang ZK, Li J, et al. Analysis Of Nonlinear Focused Ultrasound Field With Finite Element Method. 2020 15th Symposium on Piezoelectrcity, Acoustic Waves and Device Applications (SPAWDA). 2021.DOI:10.1109/SPAWDA51471.2021.9445508.
23. Kamakura, Tomoo. Two Model Equations for Describing Nonlinear Sound Beams. Japanese Journal of Applied Physics. 2004; 43(5B):2808-12. DOI:10.1143/JJAP.43.2808.
24. Mohammadpour M, Firoozabadi B. High intensity focused ultrasound (HIFU) ablation of porous liver: Numerical analysis of heat transfer and hemodynamics. Applied Thermal Engineering. 2020; 170:115014. DOI: 10.1016/j.applthermaleng.2020.115014.
25. Gupta P, Srivastava A. Non-Fourier transient thermal analysis of biological tissue phantoms subjected to high intensity focused ultrasound. International Journal of Heat and Mass Transfer. 2019; 136(7):1052-63. DOI: 10.1016/j.ijheatmasstransfer.2019.03.014.
26. Adams M T, Giraud D S, Cleveland R O. Modeling acousto-optic sensing of high-intensity focused ultrasound lesion formation. The Journal of the Acoustical Society of America. 2012; 132(3):1918. DOI:10.1121/1.4755039.
27. Sapareto SA, Dewey WC. Thermal dose determination in cancer therapy. International Journal of Radiation Oncology Biology Physics. 1984, 10(6):787-800. DOI: 10.1016/0360-3016(84)90379-1.
28. Qi M, Liu J, Mao Y. Temperature rise induced by an annular focused transducer with a wide aperture angle in multi-layer tissue. Chinese Physics B. 2018; 01(27):394-9. DOI: 10.1088/0256-307X/30/7/074302.
29. Heikkilae J, Curiel L, Hynynen K. Local Harmonic Motion Monitoring of focused Ultrasound Surgery-A Simulation Model. IEEE Transactions on Biomedical Engineering. 2010; 57(1):185-93. DOI:10.1063/1.3131411.
30. Almekkaway M K, Shehata I A, Ebbini E S. Anatomical-based model for simulation of HIFU-induced lesions in atherosclerotic plaques. International Journal of Hyperthermia the Official Journal of European Society for Hyperthermic Oncology North American Hyperthermia Group. 2015; 31(4):433-42. DOI:10.3109/02656736.2015.1018966.
31. Kyriakou Z, Corral-Baques M I, Amat A. HIFU-Induced Cavitation and Heating in Ex Vivo Porcine Subcutaneous Fat. Ultrasound in Medicine & Biology. 2011; 37(4):568-79. DOI:10.1016/ j.ultrasmedbio.2011.01.001.
32. Ginter S. Numerical simulation of ultrasound-thermotherapy combining nonlinear wave propagation with broadband soft-tissue absorption. Ultrasonics. 2000; 37(10):693-6. DOI:10.1016/S0041- 624X(00)00012-3.
33. Suomi V,Treeby B ,Jaros J. Transurethral ultrasound therapy of the prostate in the presence of calcifications: A simulation study. Medical

physics.2018;45(11):4793-805. DOI:10.1002/mp.13183.
34. Wang M, Zhou Y. High-Intensity focused Ultrasound (HIFU) Ablation by the Frequency Chirp Excitation: Reduction of the Grating Lobe in Axial focal Shifting. Journal of Physics D Applied Physics. 2018;51(28):285402. DOI:10.1088/1361-6463/aacaed.
35. Marquet F, Pernot M, Aubry J F. Non-invasive transcranial ultrasound therapy based on a 3D CT scan: protocol validation and in vitro results. Physics in Medicine & Biology. 2009; 54(9):2597-613. DOI:10.1088/0031-9155/54/9/001.
36. Aubry J, Pernot M, Marquet F. Transcostal high-intensity-focused ultrasound: ex vivo adaptive focusing feasibility study. Physics in Medicine & Biology. 2010; 53(11):2937-51. DOI: 10.1088/0031-9155/53/11/012.
37. Kyriakou A, Neufeld E, Werner B. A review of numerical and experimental compensation techniques for skull-induced phase aberrations in transcranial focused ultrasound. International Journal of Hyperthermia. 2014; 30(1):36-46. DOI:10.3109/02656736.2013.861519.
38. Casarotto R A, Adamowski J C, Fallopa F. Coupling agents in therapeutic ultrasound: acoustic and thermal behavior. Archives of Physical Medicine & Rehabilitation. 2004; 85(1):162-5. DOI:10.1016/S0003-9993(03)00293-4.
39. Balmaseda MT, Fatehi MT, Koozekanani SH. Ultrasound therapy: a comparative study of different coupling media. Archives of Physical Medicine and Rehabilitation. 1986; 67(3):147-50.
40. Sites B D, Brull R, Chan V. Artifacts and pitfall errors associated with ultrasound-guided regional anesthesia. Part I: understanding the basic principles of ultrasound physics and machine operations. Reg Anesth Pain Med. 2007; 32(5):412-8. DOI: 10.1016/j.rapm.2007.05.005.
41. WD O′Brien. Ultrasound-biophysics mechanisms. Prog Biophys Mol Biol. 2007; 93(1-3):212-55. DOI: 10.1016/j.pbiomolbio.2006.07.010.
42. Tharkar P, Varanasi R, Wu S. Nano-Enhanced Drug Delivery and Therapeutic Ultrasound for Cancer Treatment and Beyond. Frontiers in Bioengineering and Biotechnology. 2019; 7. DOI: 10.3389/fbioe.2019.00324.
43. Yan S, Min L U, Ding X. HematoPorphyrin Monomethyl Ether polymer contrast agent for ultrasound/photoacoustic dual-modality imaging-guided synergistic high intensity focused ultrasound (HIFU) therapy. Scientific Reports. 2016; 6:31833. DOI:10.1038/srep31833.
44. Ogbole GI. Radiation dose in paediatric computed tomography: risks and benefits. Annals of Ibadan postgraduate medicine. 2010;8 (2):118-26.